

Lévy sources in UrQMD in Ar+Sc collisions at SPS energies

Barnabás Pórfy^{1,2} and Máté Csanád¹

¹Department of Atomic Physics, ELTE Eötvös Loránd University, Budapest, Hungary

²HUN-REN Wigner Research Centre for Physics, Budapest, Hungary

December 5, 2025

Abstract

Over the past few decades, progress in femtoscopy has been driven by the interplay between experimental measurements and theoretical calculations. Measurements provide data for the theory to understand it, while theoretical predictions guide new measurements. In the recent decade, several experiments have confirmed that the two-particle pion emitting source is well described by Lévy alpha-stable distributions. To enable theoretical interpretation, phenomenological simulations have been done at RHIC and LHC energies, using various available heavy-ion collision models. In this paper, we investigate three-dimensional two-pion pair source distributions from $^{40}\text{Ar}+^{45}\text{Sc}$ central collisions at SPS energies, generated with the Ultra-Relativistic Quantum Molecular Dynamics Monte-Carlo event generator. We fit the pair source with Lévy-stable distributions, and discuss the extracted Lévy parameters describing the spatial scale, shape and strength of the source.

1 Introduction

The general goal of high-energy heavy-ion experiments is to explore the properties of the strongly interacting matter created in heavy-ion collisions. A key objective is to understand the space-time geometry of the particle-emitting source. One approach to this is femtoscopy, i.e., the analysis of quantum-statistical correlations of particles produced in such collisions [1, 2]. Experimental results based on the so-called imaging technique [3] around the turn of the millennium [4], together with more recent measurements [5–9], indicate that the commonly assumed Gaussian shape of the source [10, 11] does not provide an adequate description. Instead, the two-pion source function exhibits a power-law tail, and a Lévy-type parametrization offers a statistically robust description of the measured femtoscopic correlation functions across collision energies. [12]

Several physical mechanisms may contribute to the appearance of Lévy distributions in high-energy heavy-ion collisions. Lévy walk has been shown to play a major role [13] in generating Lévy-distributed sources [14] due to the generalized central limit theorem and anomalous diffusion [15], and it was also demonstrated that directional and event averaging in experimental analyses does not influence this behavior [16–18]. Additional possible sources of Lévy-type emission patterns include jet fragmentation [19] and critical dynamics near the QCD critical point [20]. To investigate these underlying processes, phenomenological studies with event generators are particularly valuable. An available option is to use the Ultra-Relativistic Quantum Molecular Dynamics (UrQMD) framework [21, 22]. The clear advantage of using such event generators is the direct reconstruction of the source function; therefore, hidden properties of experimental data may be uncovered by investigating simulated events.

In this paper, we present a detailed investigation of the two-particle source function using like-charged pions in argon–scandium ($^{40}\text{Ar}+^{45}\text{Sc}$) collision data at the available energy range of the NA61/SHINE experiment [23] ($\sqrt{s_{\text{NN}}} \approx 5\text{--}17 \text{ GeV}$, or $13\text{--}150\text{A}$ GeV/c beam momentum) generated by the UrQMD model. The reconstructed two-particle source functions are fitted with three-dimensional Lévy distributions, similarly to Ref. [18]. The source parameters are studied as functions of pair transverse mass and collision energy.

The paper is structured as follows: In Sec. 2, the properties of the two-particle source function are detailed alongside the Lévy approach and the event generator, and the following Sec. 3 gives the details on the measurement and analysis itself. The results of Lévy parameters as a function of transverse mass as well as a function of collision energy are detailed in Sec. 4. Finally, the conclusions are presented in Sec. 5.

2 Two-particle source function

The investigation of quantum-statistical correlation functions is one of the most important methods in heavy-ion physics. Femtoscopic correlations provide information about the space-time geometry of the particle-emitting

source [24, 25]. The connection between the two-particle momentum correlations (C_2) and the pair source distribution (D) is as follows:

$$C_2(q, K) = \int d^4 r D(r, K) |\Psi_q^{(2)}(r)|^2, \quad (1)$$

where $q = p_1 - p_2$ is the momentum difference of the pair, $K = (p_1 + p_2)/2$ signifies the average pair momentum and $r = x_1 - x_2$ denotes the four vector distance of the pair, while $\Psi_q^{(2)}(r)$ is the pair wave function. Thus, through measuring the correlation function, femtoscopy maps the pair source distribution and the pair wave function. The pair source is the autocorrelation of single-particle source functions (S) and is introduced as

$$D(r, K) = \int d^4 \sigma S(\sigma + r/2, K) S(\sigma - r/2, K), \quad (2)$$

where $\sigma = (x_1 + x_2)/2$ is the pair center of mass. It is important to note that in both Eq. (1) and Eq. (2) the dependence on K is assumed to be weaker [24] and is often appears only through the dependence of parameters on it. While for the shape of the source, historically a Gaussian was assumed [11], a more general approach is a three-dimensional Lévy-stable distribution [14]

$$\mathcal{L}(\alpha, R^2, \vec{r}) = \frac{1}{(2\pi)^3} \int d^3 \vec{\zeta} e^{i\vec{\zeta} \cdot \vec{r}} e^{-\frac{1}{2} |\vec{\zeta}^T R^2 \vec{\zeta}|^{\alpha/2}}. \quad (3)$$

where the parameters of this distribution are α , the Lévy stability index, and the R^2 matrix of Lévy scale parameters or radii, often assumed to be diagonal, i.e., $\text{diag}(R_{\text{out}}^2, R_{\text{side}}^2, R_{\text{long}}^2)$ in the Bertsch–Pratt coordinate system [26, 27]. Furthermore, \vec{r} is the vector of spatial coordinates, and the vector $\vec{\zeta}$ represents the integration variable. In the case of $\alpha = 2$, one recovers the Gaussian distribution, while $\alpha = 1$ is equivalent to the Cauchy distribution, and for $\alpha < 2$, the Lévy distribution exhibits a power-law tail. The defining “stability” property of these distributions is that they retain the same shape parameter under convolution. Consequently, if single particle sources are Lévy distributed, the pair source distribution is also Lévy shaped with the same α value, and Lévy radii are scaled by a factor of $2^{1/\alpha}$ [5].

As stated in the introduction, experimental heavy-ion physics has limited access to the exact freeze-out coordinates of hadrons, i.e. to the pair source distribution. On the other hand, in event generators one may get access to it. One such generator is the UrQMD framework [21, 22], detailed in the following part.

3 Analysis details

3.1 UrQMD

The UrQMD event generator is a microscopic transport model widely used to simulate heavy-ion collisions over a broad range of energies. The model is well suited to be applied in the 2–160A GeV beam energy region, in line with the energy range available at the NA61/SHINE experiment [23]. We employ the UrQMD model (v3.4) in cascade mode as the main event generator. For this study, UrQMD was slightly altered to include the decay of η mesons, based on the work detailed in [28], in order to improve the connection to real data. However, this only affects the strength of the extracted source.

Simulations were performed for beam momenta of 13–150A GeV/ c in the ${}^{40}\text{Ar}+{}^{45}\text{Sc}$ collision system, corresponding to center of mass energies per nucleon pair of $\sqrt{s_{\text{NN}}} \approx 5\text{--}17$ GeV. For each energy, 10,000 events were generated in the 0–10% centrality range with time evolution duration set to 10,000 fm/ c . To align with the experimental analyses, centrality selection was defined by assessing the total energy in the kinematical range of the Projectile Spectator Detector (PSD) used for centrality selection in the NA61/SHINE experiment, detailed in [23]. Events with the smallest amount of PSD-range energy (E_{PSD}) can be considered most central. The E_{PSD} limit for 0–10% centrality range was then determined based on Minimum Bias UrQMD simulations.

3.2 Pair source function

The choice of frame is essential for femtoscopy studies, and two options are often chosen: the pair center of mass system (PCMS) and the longitudinally comoving system (LCMS). In case of the PCMS, the total three-momentum vanishes. On the other hand, in the LCMS frame, for mid-rapidity measurements the cross-terms will vanish [29, 30], rendering the source nearly spherically symmetric [5]. In the LCMS, the longitudinal component (beam direction) of the pair average momentum is zero by definition. Additionally, one often uses the Bertsch–Pratt coordinate system [26, 31], where “long” corresponds to the aforementioned longitudinal direction, “out” direction is the direction of the average pair momentum perpendicular to “long”. Finally, “side”

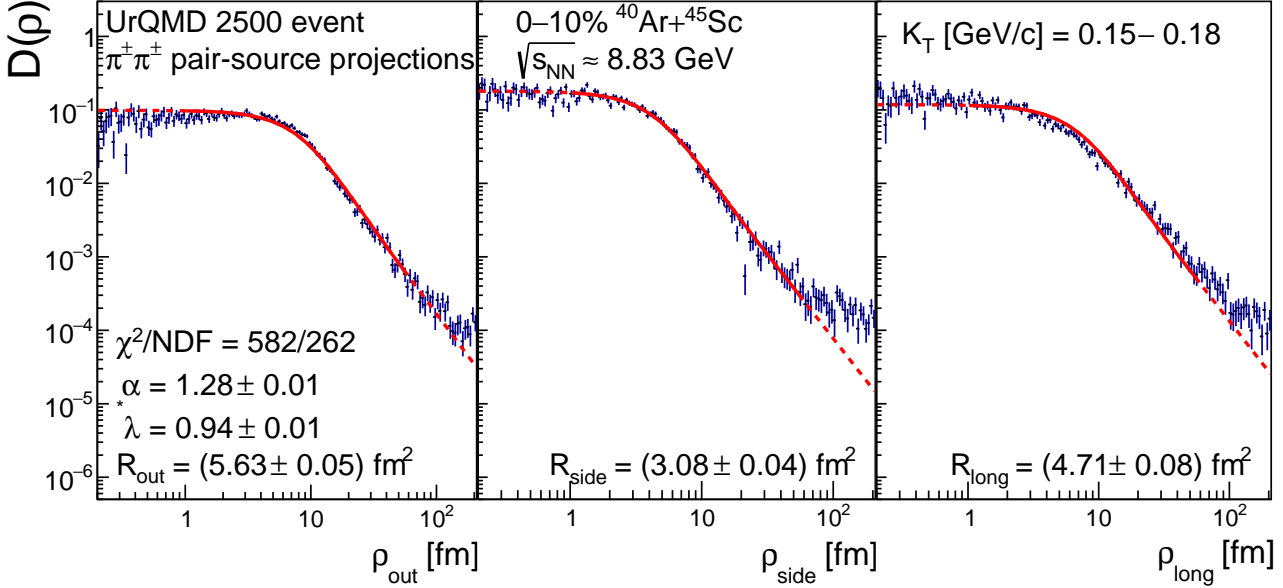


Figure 1: Example fit (red line) to projected $D(\rho)$ distributions (blue points) in Ar+Sc 0-10% centrality at $40A$ GeV/c in K_T range [0.15-0.18] GeV/c with 2500 events merged. The fit is marked with a solid line, while the dashed line is an extrapolation.

is perpendicular to both directions. To access the pair source function, we follow the definition of Ref. [13] for the three-dimensional spatial distance vector (in $c = 1$ units):

$$\vec{\rho} = \vec{r} - \frac{\vec{K}}{K_0} t. \quad (4)$$

Its components in the LCMS can be expressed from lab-frame coordinates and momenta as [13]

$$\rho_{\text{out}}^{\text{LCMS}} = r_x \cos \varphi + r_y \sin \varphi - \frac{K_T}{K_0^2 - K_z^2} (K_0 t - K_z r_z) \quad (5)$$

$$\rho_{\text{side}}^{\text{LCMS}} = -r_x \sin \varphi + r_y \cos \varphi \quad (6)$$

$$\rho_{\text{long}}^{\text{LCMS}} = \frac{K_0 r_z - K_z t}{\sqrt{K_0^2 - K_z^2}}, \quad (7)$$

where $\cos \varphi = K_x / K_T$, $\sin \varphi = K_y / K_T$, and $K_T^2 = K_x^2 + K_y^2$.

In this analysis, we calculate the one-dimensional projections of the three-dimensional $D(\vec{\rho})$ distribution:

$$D(\rho_{\text{out}}^{\text{LCMS}}), \quad D(\rho_{\text{side}}^{\text{LCMS}}), \quad D(\rho_{\text{long}}^{\text{LCMS}}),$$

and fit them with the projections of Lévy distributions, as defined in Eq. (3). Unlike the gold-gold or lead-lead collision analyzed Refs. [16, 17], single Ar+Sc events lack sufficient statistics for this procedure, hence, similarly to Refs. [18, 32], we sum the D distributions of several events. The fit parameters converge as the number of summed events (N_{events}) increases, thus we can chose a sufficiently large N_{events} value, and then average the results from such blocks of events. As a default, we use $N_{\text{events}} = 2500$ for $p_{\text{beam}} = 150, 75$ and $40A$ GeV/c, and 5000 for $p_{\text{beam}} = 30, 19$ and $13A$ GeV/c. To create conditions similar to the experimental analysis, several kinematic cuts are also applied: pions with single-track rapidity < 1 (1.5 for $150A$ GeV/c), and with transverse momentum $p_T < 1.5$, are selected. Furthermore, to replicate the effect of the limited fit range in the experimental momentum correlation functions, we select pairs with a limited momentum difference: a $q_{\text{LCMS}} < \sqrt{m_T} \cdot 150$ MeV cut is applied. We then investigate the $D(\rho)$ distributions in eight K_T classes ranging from 0 to 1 GeV/c, similarly to the experimental analysis of Ref. [33].

3.3 Systematic Uncertainties

In the analysis, we carefully consider uncertainties as well. The statistical uncertainties depend on the number of events considered and are negligible in our case. Systematic uncertainties, on the other hand, are of high importance. To assess these, we examined several different settings to understand their impact on the data. The settings are summarized in the Table 1. The total systematic uncertainty is then calculated, based on the

Table 1: Systematic uncertainty sources, their different settings, and values for all energies.

Energy	N_{events}	$Q_{\text{LCMS}}^{\max} [\text{GeV}/c]$	Fit range [fm]		
150A GeV/c	standard: 2500 strict: 1000 loose: 5000	standard: $\sqrt{150 \text{ GeV}/c^2 \cdot m_{\text{T}}}$ strict: $\sqrt{100 \text{ GeV}/c^2 \cdot m_{\text{T}}}$ loose: $\sqrt{250 \text{ GeV}/c^2 \cdot m_{\text{T}}}$	standard: 1-60 strict: 1-40 loose: 1-80		
75A GeV/c					
40A GeV/c					
30A GeV/c	standard: 5000 strict: 2500 loose: 10000				
19A GeV/c					
13A GeV/c					

 Table 2: Average relative systematic uncertainties over all K_{T} intervals for selected energies.

p_{beam} [A GeV/c]	Source	α [%]	λ [%]	R [%]	R_{out} [%]	R_{side} [%]	R_{long} [%]
150	Q_{LCMS}^{\max}	2.20	0.90	1.01	0.75	0.52	1.44
	Fit range	1.58	1.74	2.83	2.24	3.08	3.50
	N_{events}	1.30	1.78	3.50	2.85	3.46	4.23
	Total uncertainty	3.91	3.32	5.50	4.37	5.31	6.85
40	Q_{LCMS}^{\max}	1.66	0.63	0.51	0.34	0.22	0.94
	Fit range	1.18	0.56	0.99	1.02	0.59	1.43
	N_{events}	0.61	0.24	0.24	0.18	0.14	0.37
	Total uncertainty	2.42	0.98	1.19	1.14	0.74	1.85
13	Q_{LCMS}^{\max}	1.03	0.28	0.06	0.08	0.20	0.09
	Fit range	0.47	0.22	0.67	0.76	0.41	1.17
	N_{events}	0.32	0.09	0.02	0.02	0.05	0.07
	Total uncertainty	1.40	0.43	0.68	0.79	0.50	1.20

default value ($P_{\text{i}}^{\text{def}}$) of a parameter, its varied value ($P_{\text{i}}^{\text{var}}$) for the i th source (among the $n = 3$ sources: N_{events} , Q_{LCMS}^{\max} , fit range), separately for the positive and negative uncertainties ($j = +, -$):

$$\sigma_{i,j}^2[P] = (P_{\text{i}}^{\text{def}} - P_{\text{i},j}^{\text{var}})^2 \quad (8)$$

$$\sigma_j^{\text{tot}}[P] = \sqrt{\sum_{i=1}^n \sigma_{i,j}^2[P]}. \quad (9)$$

This total uncertainty $\sigma_{\pm}^{\text{tot}}$ is subsequently shown on the results as an uncertainty band. The averaged systematic uncertainty for three energies are summarized in Table 2.

4 Results

Let us now turn towards the extracted fit parameters. Fig. 2a shows the Lévy index α as a function of m_{T} for all simulated beam momenta (collision energies). It is apparent that α has a moderate dependence on m_{T} : a slight increase with m_{T} is observable for all collision energies. Furthermore, a point-by-point decrease of $\alpha(m_{\text{T}})$ with collision energy is visible. To investigate this, α versus $\sqrt{s_{\text{NN}}}$ is shown in Fig. 2b in three selected (low, medium, and high) m_{T} intervals. The collision energy dependence is qualitatively similar at all transverse momenta, but clear quantitative differences are observable. In particular, at the lowest m_{T} , α versus $\sqrt{s_{\text{NN}}}$ rapidly decreases to a value around unity and appears to flatten out, while for the highest m_{T} a smooth and continuous decrease is observable. To further investigate the overall trends, the m_{T} -averaged $\langle \alpha \rangle$ is shown as a function of collision energy ($\sqrt{s_{\text{NN}}}$) in Fig. 2c, where the decreasing trend with increasing energy is observable. This is in contrast to preliminary NA61/SHINE data [33] where an opposite trend was seen, with an additional approximate minimum at around $\sqrt{s_{\text{NN}}} \approx 6 - 8$ GeV.

Fig. 3 shows the intercept parameter, or correlation strength parameter λ^* . We denote this parameter with an additional $*$, as in UrQMD, even after modifying the code to include the decays of the η meson, several weak decays are not included (those of kaons, Σ , Ω , Ξ baryons), and henceforth the pions stemming from the decays of these particles are missing from our simulation. These pions would all contribute to the halo (except for those from charged kaons, as these are produced so far out that they are removed from the pion sample in most experimental settings), thus our calculations result in a larger correlation strength. Therefore direct comparison to λ measurements is not possible. On the other hand, one can estimate the effect of the missing weak decays by calculating how many pions would have been produced had the above particles decayed, taking branching ratios also into account. We find that the “true” λ would be about 92%-93% of the obtained value if these decays were incorporated (this fraction decreases very slowly with collision energy in the 13A-150A GeV/c range). This correction aside, investigating the λ^* versus m_{T} behavior, a small increase is found, while no clear collision energy dependence emerges.

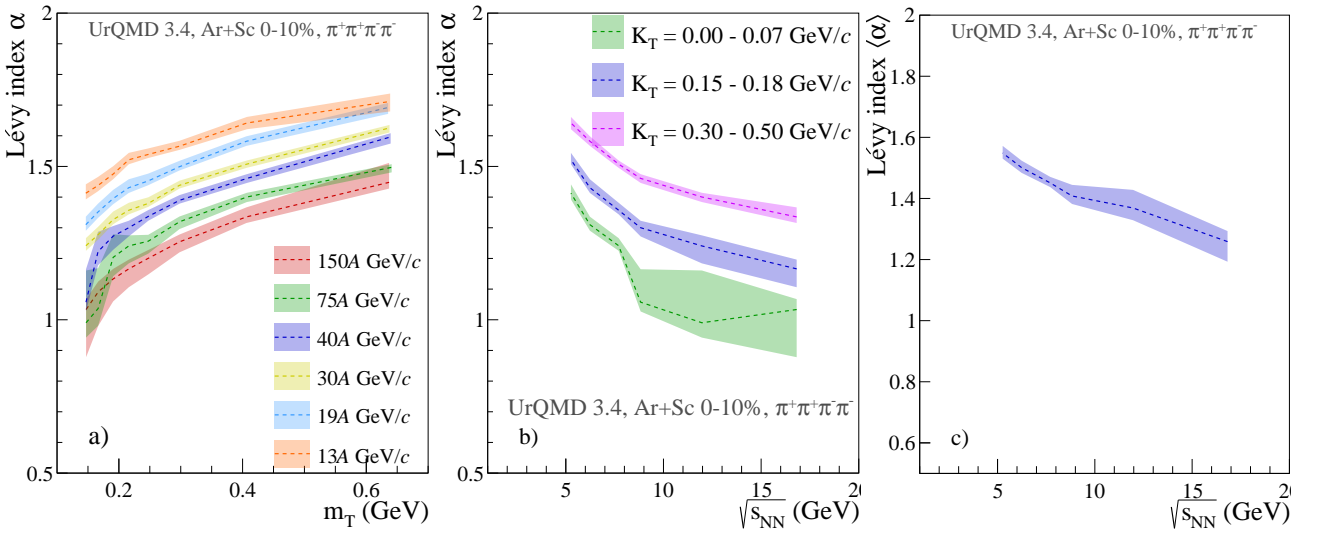


Figure 2: The Lévy index parameter α , for 0–10% central Ar+Sc. For all transverse mass m_T a), for selected transverse mass m_T intervals b), and the average of all transverse mass m_T intervals at the given energies c). The given colored band shows systematic uncertainty.

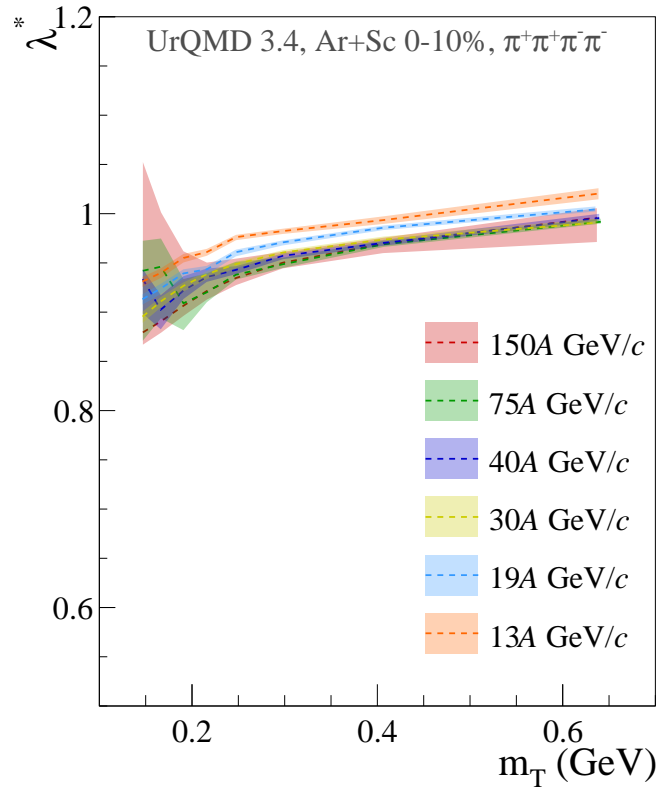


Figure 3: The intercept parameter λ^* , for 0–10% central Ar+Sc at all beam momenta, as a function of transverse mass m_T . The given colored band shows systematic uncertainty.

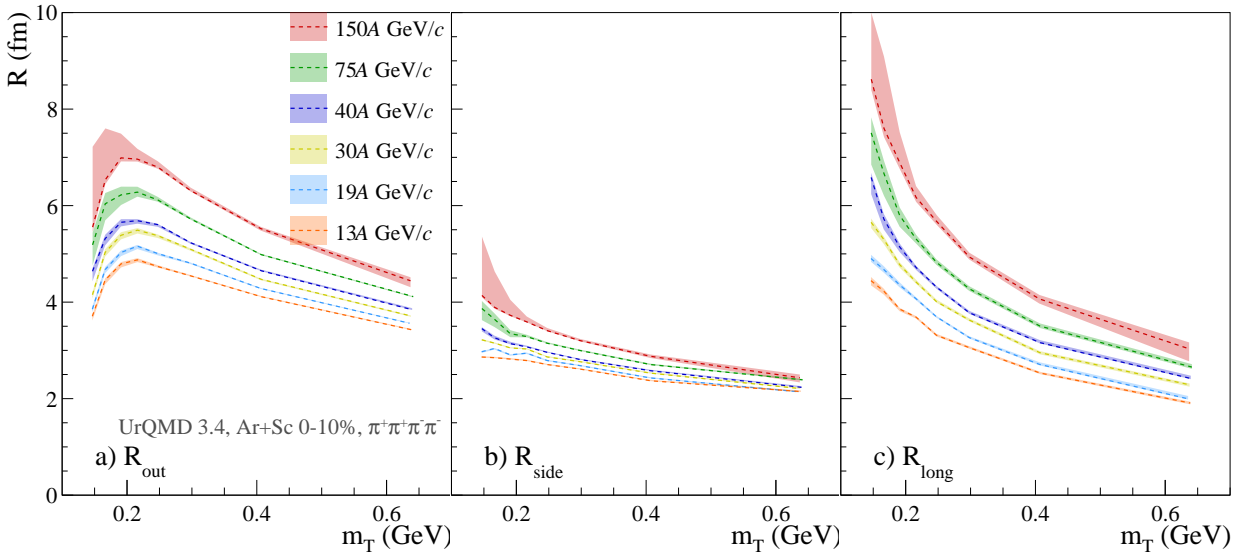


Figure 4: The Lévy-scale parameters R_{out} , R_{side} , R_{long} , for 0–10% central Ar+Sc at all beam momenta, as a function of transverse mass m_T . The colored bands show the systematic uncertainty.

Fig. 4 shows the Lévy scale parameters R_{out} , R_{side} , and R_{long} . In all three directions, a clear decreasing trend with m_T is observed, as traditionally attributed to an expanding source [30], and observed in hydrodynamic models as well [34]. On the other hand, several differences can be identified in terms of exact trends and values. Notably, in the “out” direction in the very low transverse mass regions, for all energies, a small maximum appears at around 0.2 GeV. There is also a clear ordering of the parameters at low m_T : radii are decreasing in the order of “long”, “out”, “side”, while this ordering changes at higher m_T values: the longitudinal scale becomes almost as small as the “side” one. To compare with one-dimensional femtoscopic analyses, it is also important to investigate the average $\bar{R} = \sqrt{(R_{\text{out}}^2 + R_{\text{side}}^2 + R_{\text{long}}^2)/3}$, shown as a function of m_T in Fig. 5a. Fig. 5b shows the collision energy dependence of the radii in three K_T intervals. These exhibit a similar increase; however, their trends are slightly different, especially in the case of the lowest K_T bin, similarly to the case of $\langle \alpha \rangle$.

5 Conclusion

We investigated two-pion spatial pair distance distributions in three dimensions, based on 10,000 Ar+Sc 0–10% centrality collisions per collision energy, generated in the UrQMD framework at beam momenta 13, 19, 30, 40, 75, and 150A GeV/c. The pair distance distributions for pions were directly calculated on an event-by-event basis. For the subsequent analysis distributions from a predefined number of events were added to ensure sufficient statistics, as well as convergence of the parameters. The three-dimensional Lévy-stable distributions were found to describe the simulated data. The Lévy source parameters were investigated as a function of transverse mass and collision energy. It was found that the Lévy index α shows a moderate but clear increase with transverse mass, and a decrease with collision energy. For the Lévy scale parameters, a decreasing trend with transverse mass and a clear increase with collision energy was found. Furthermore, the correlation strength parameter λ was also investigated, and no clear trends with energy were observed, but a small increase with transverse mass was found. However, in our framework, due to the lack of weak decays of particles such as K_S^0, Λ in UrQMD, a 7 – 8% larger λ is extracted by definition. Altogether, these results form an important baseline when compared to future experimental studies, as well as simulations of various collision systems and energies.

6 Acknowledgments

This research was funded by the NKFIH grants TKP2021-NKTA-64, PD-146589, K-146913, K-138136, and NKKP-152097. Barnabás Pörfy furthermore acknowledges support of the DKOP-23 Doctoral Excellence Program of the Ministry for Culture and Innovation.

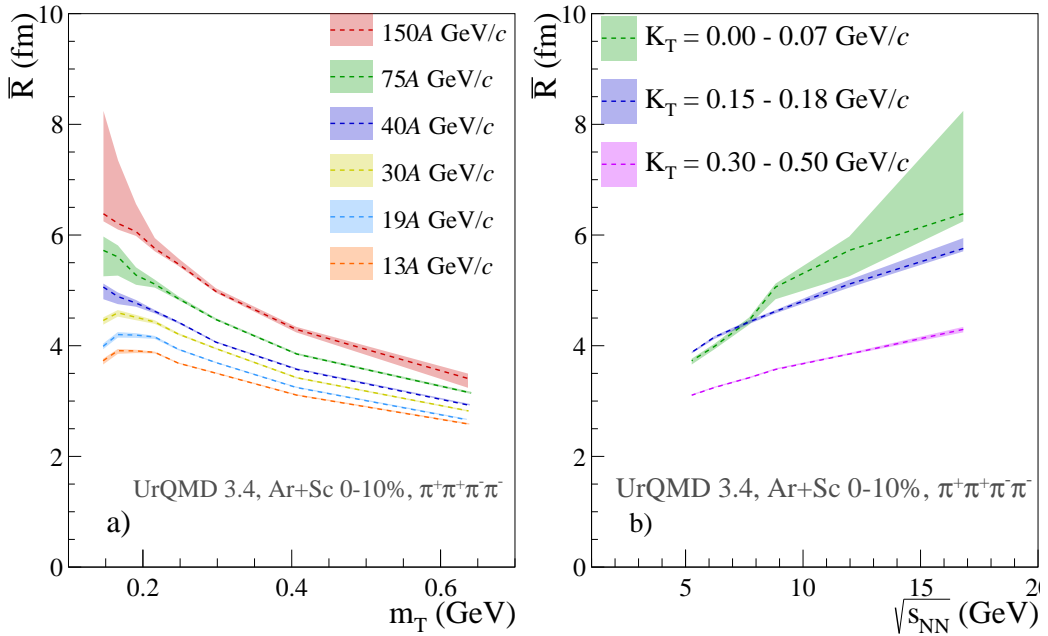


Figure 5: The averaged Lévy-scale parameter \bar{R} , for 0–10% central Ar+Sc. For all transverse mass m_T as a function of m_T a) and for selected transverse mass m_T intervals as a function of beam momentum b). The given colored band shows systematic uncertainty.

References

- [1] G. Goldhaber, W. B. Fowler, S. Goldhaber, and T. F. Hoang. Pion-pion correlations in antiproton annihilation events. *Phys. Rev. Lett.*, 3:181, 1959.
- [2] G. Goldhaber, S. Goldhaber, W.-Y. Lee, and A. Pais. Influence of Bose-Einstein statistics on the anti-proton proton annihilation process. *Phys. Rev.*, 120:300, 1960.
- [3] D. A. Brown and P. Danielewicz. Imaging of sources in heavy ion reactions. *Phys. Lett. B*, 398:252–258, 1997.
- [4] S. S. Adler et al. Evidence for a long-range component in the pion emission source in Au + Au collisions at $\sqrt{s_{NN}} = 200$ GeV. *Phys. Rev. Lett.*, 98:132301, 2007.
- [5] A. Adare et al. Lévy-stable two-pion Bose-Einstein correlations in $\sqrt{s_{NN}} = 200$ GeV Au+Au collisions. *Phys. Rev. C*, 97(6):064911, 2018. [Erratum: Phys.Rev.C 108, 049905 (2023)].
- [6] H. Adhikary et al. Two-pion femtoscopic correlations in Be+Be collisions at $\sqrt{s_{NN}} = 16.84$ GeV measured by the NA61/SHINE at CERN. *Eur. Phys. J. C*, 83(10):919, 2023.
- [7] A. Tumasyan et al. Two-particle Bose-Einstein correlations and their Lévy parameters in PbPb collisions at $s_{NN}=5.02$ TeV. *Phys. Rev. C*, 109(2):024914, 2024.
- [8] D. Kincses. Pion Interferometry with Lévy-Stable Sources in = 200 GeV Au + Au Collisions at STAR. *Universe*, 10(3):102, 2024.
- [9] N. J. Abdulameer et al. Centrality dependence of Lévy-stable two-pion Bose-Einstein correlations in $s_{NN}=200$ GeV Au+Au collisions. *Phys. Rev. C*, 110(6):064909, 2024.
- [10] T. Csörgő, B. Lorstad, and J. Zimányi. Quantum statistical correlations for slowly expanding systems. *Phys. Lett. B*, 338:134–140, 1994.
- [11] S. V. Akkelin and Yu. M. Sinyukov. The HBT interferometry of expanding sources. *Phys. Lett. B*, 356:525–530, 1995.
- [12] M. Csanad and D.I Kincses. Femtoscopy with Levy Sources from SPS through RHIC to LHC. *Universe*, 10(2):54, 2024.

[13] Dániel Kincses, Márton Nagy, and Máté Csanád. Lévy walk of pions in heavy-ion collisions. *Commun. Phys.*, 8(1):55, 2025.

[14] T. Csorgo, S. Hegyi, and W. A. Zajc. Bose-Einstein correlations for Levy stable source distributions. *Eur. Phys. J. C*, 36:67–78, 2004.

[15] M. Csanad, T. Csorgo, and M. Nagy. Anomalous diffusion of pions at RHIC. *Braz. J. Phys.*, 37:1002–1013, 2007.

[16] D. Kincses, M. Stefaniak, and M. Csanád. Event-by-Event Investigation of the Two-Particle Source Function in Heavy-Ion Collisions with EPOS. *Entropy*, 24(3):308, 2022.

[17] B. Kórodi, D. Kincses, and M. Csanád. Event-by-event investigation of the two-particle source function in sNN=2.76 TeV PbPb collisions with EPOS. *Phys. Lett. B*, 847:138295, 2023.

[18] D. Kincses, E. Árpási, L. Kovács, M. Nagy, and M. Csanád. Three-dimensional sizes and shapes of pion emission in heavy-ion collisions. 11 2025.

[19] T. Csörgő, S. Hegyi, T. Novak, and W. A. Zajc. Bose-Einstein or HBT correlations and the anomalous dimension of QCD. *Acta Phys. Polon. B*, 36:329–337, 2005.

[20] T. Csörgő, S. Hegyi, T. Novák, and W. A. Zajc. Bose-Einstein or HBT correlation signature of a second order QCD phase transition. *AIP Conf. Proc.*, 828(1):525–532, 2006.

[21] S.A. Bass et al. Microscopic models for ultrarelativistic heavy ion collisions. *Prog. Part. Nucl. Phys.*, 41:255–369, 1998.

[22] M. Bleicher et al. Relativistic hadron hadron collisions in the ultrarelativistic quantum molecular dynamics model. *J. Phys.*, G25:1859–1896, 1999.

[23] N. Abgrall et al. NA61/SHINE facility at the CERN SPS: beams and detector system. *JINST*, 9:P06005, 2014.

[24] M. A. Lisa, S. Pratt, R. Soltz, and U. Wiedemann. Femtoscopy in relativistic heavy ion collisions. *Ann. Rev. Nucl. Part. Sci.*, 55:357–402, 2005.

[25] T. Csörgő. Particle interferometry from 40-MeV to 40-TeV. *Acta Phys. Hung. A*, 15:1–80, 2002.

[26] G. Bertsch, M. Gong, and M. Tohyama. Pion Interferometry in Ultrarelativistic Heavy Ion Collisions. *Phys. Rev. C*, 37:1896–1900, 1988.

[27] S. Pratt, T. Csörgő, and J. Zimányi. Detailed predictions for two pion correlations in ultrarelativistic heavy ion collisions. *Phys. Rev. C*, 42:2646–2652, 1990.

[28] V. Uzhinsky. Toward UrQMD Model Description of pp and pC Interactions at High Energies. 8 2013.

[29] Scott Chapman, Pierre Scotto, and Ulrich W. Heinz. A New cross term in the two particle HBT correlation function. *Phys. Rev. Lett.*, 74:4400–4403, 1995.

[30] S. S. Adler et al. Bose-Einstein correlations of charged pion pairs in Au + Au collisions at $s(\text{NN})^{**}(1/2) = 200\text{-GeV}$. *Phys. Rev. Lett.*, 93:152302, 2004.

[31] S. Pratt. Coherence and Coulomb Effects on Pion Interferometry. *Phys. Rev. D*, 33:72–79, 1986.

[32] Yan Huang, Matyas Molnar, Daniel Kincses, and Mate Csanad. Excitation function of femtoscopic Lévy source parameters of pion pairs in EPOS4. 12 2025.

[33] B. Pórfy. Femtoscopy using Lévy-type source at NA61/SHINE. *PoS*, ICHEP2024:603, 2025.

[34] T. Csörgő and B. Lörstad. Bose-Einstein correlations for three-dimensionally expanding, cylindrically symmetric, finite systems. *Phys. Rev. C*, 54:1390–1403, 1996.